SCIENTIFIC REP⚙RTS

A lumenal interrupted helix in human sperm tail microtubules

Davide Zabeo[1], John M. Heumann[2], Cindi L. Schwartz[2], Azusa Suzuki-Shinjo[3], Garry Morgan[2], Per O. Widlund[4] & Johanna L. Höög[1]

Eukaryotic flagella are complex cellular extensions involved in many human diseases gathered under the term ciliopathies. Currently, detailed insights on flagellar structure come mostly from studies on protists. Here, cryo-electron tomography (cryo-ET) was performed on intact human spermatozoon tails and showed a variable number of microtubules in the singlet region (inside the end-piece). Inside the microtubule plus end, a novel left-handed interrupted helix which extends several micrometers was discovered. This structure was named Tail Axoneme Intra-Lumenal Spiral (TAILS) and binds directly to 11 protofilaments on the internal microtubule wall, in a coaxial fashion with the surrounding microtubule lattice. It leaves a gap over the microtubule seam, which was directly visualized in both singlet and doublet microtubules. We speculate that TAILS may stabilize microtubules, enable rapid swimming or play a role in controlling the swimming direction of spermatozoa.

Cilia and flagella can be found on many animal, plant and protist cells. It is an important cellular structure that can either act as an antenna[1], receiving signals from the environment, or provide cellular motility, such as in sperm tails. Malfunctions of human cilia and flagella are known as ciliopathies, and diseases of the motile cilium specifically are called primary ciliary dyskinesia (PCD). Patients with PCD present variable symptoms, such as pulmonary disease, situs inversus and infertility in both males and females[2,3].

The flagellum consists of a membrane-covered axoneme, a complex arrangement of nine doublet microtubules (dMTs) surrounding two singlet central pair microtubules (CPs; the $9 + 2$ arrangement), interlinked with a multitude of protein complexes[4]. The dMTs consist of one complete A-tubule, made of 13 protofilaments, and a B-tubule, with 10 protofilaments[5]. In a complete microtubule made of 13 protofilaments, each α and β tubulin subunit is laterally adjacent and longitudinally offset to another subunit of its same kind. The only exception occurs at the seam, where an α and a β tubulin subunits are laterally in contact[6–8]. This feature is part of the common lattice of each single microtubule. It is currently unclear where the seam is located in axonemal microtubules. The location of this seam in the A-tubule has been suggested to be both at the dMT inner junction[9] and outer junction[10,11]. Close to the distal tip of the eukaryotic flagellum, the B-tubule of dMTs often terminates and the A-tubule continues on, forming the so called "singlet zone"[12,13]. However, the presence of this singlet zone and its extent vary greatly between species[13–15]. Sperm tails consists of three major parts: the mid piece where the mitochondrion is wrapped around the tail, the principal piece where a complete $9 + 2$ axoneme is surrounded by 9 sperm-specific outer dense fibers and a fibrous sheet, and finally the terminus or end-piece. In spermatozoa, the singlet zone is contained within the end-piece. In rodent sperm, Woolley and Nickels (1985) observed that both the A-tubule and the B-tubule can transition into singlet microtubules at the flagellum tip, coining the term "duplex microtubules" for this singlet region arrangement[16]. These duplex microtubules were later also identified in human spermatozoa[3].

Microtubules are regulated by hundreds of microtubule-associated proteins (MAPs) and motor proteins[17–19]. MAPs fall into several categories based on their functions but, with regards to localization, they are classified into three main groups: those that bind the more dynamic plus end (+TIPs), e.g. EB1, XMAP215 and CLIP1[20–22], those that bind and often stabilize the minus end, e.g. gamma tubulin and patronin[23–25], and those that more generally interact with the microtubule outer surface, e.g. PRC1[26,27]. Motor proteins can be found at all three locations, depending on the polarity of their movement[28]. Altogether, in any given cell, the microtubule outer

[1]Department of Chemistry and Molecular Biology, University of Gothenburg, Gothenburg, 41390, Sweden. [2]Department of Molecular, Cellular and Developmental Biology, University of Colorado, Boulder, CO, 80309, USA. [3]Krefting Research Centre, University of Gothenburg, Gothenburg, 41390, Sweden. [4]Sahlgrenska Academy, University of Gothenburg, Gothenburg, 41390, Sweden. Correspondence and requests for materials should be addressed to J.L.H. (email: johanna.hoog@gu.se)

Number of cryo-ETs	55
Number of cells imaged	33
Number of cryo-ETs used in sub-ET average:	
- singlet MTs	3
- doublet MTs	1
Number of particles used in sub-ET average:	
- singlet MTs	1940
- doublet MTs	478

Table 1. Number of electron tomograms acquired, cells imaged and sub-tomograms used for averaging.

surfaces, plus and minus ends are often occupied by a wide assortment of MAPs and motor proteins that affect their characteristics, likely exerting effects through synergistic ways[29,30].

Only two known MAPs, tau and tubulin acetylase, have been suggested to localize in the microtubule interior[31,32]. Yet, electron microscopy and (cryo) electron tomography have shown that proteins also localize to the inside of microtubules[33–41]. These microtubule inner proteins (MIPs) are often found in dMTs and are all of unknown identity and function. However, their specific localization and variable frequency suggest that they serve important regulatory functions for the microtubule cytoskeleton[5].

In this study, we performed the first three-dimensional reconstruction of intact human flagella using cryo-electron tomography on spermatozoon tails. By visualizing this cell type, we discovered a novel protein complex, Tail Axoneme Intra-Lumenal Spiral (TAILS), spanning several micrometers in the lumens of all healthy human spermatozoa axonemal microtubules at the distal end. TAILS binds to the inside of the microtubule and leaves a gap over the seam. The sub-tomogram average achieved sufficient resolution to resolve the tubulin subunits and the microtubule seam was directly visualized.

Results

Observation of an interrupted helix in the singlet microtubule lumen.
To study the structure of human flagella, we performed cryo-electron microscopy of the distal tip of human spermatozoa that were plunge-frozen in complete seminal fluid and we generated 55 cryo-electron tomograms on a total of 33 different intact human sperm tails (Table 1). The exact location along the sperm tails and area included in 22 of those tomograms could be identified using lower magnification images (Fig. 1A).

The end piece of spermatozoa contained only singlet microtubules (Fig. 1B,C). Twenty-three cryo-electron micrographs of different human spermatozoa end pieces displayed an unexpected, extensive, and regular interior structure in all microtubules (Supplementary Figure 1). This structure was further analyzed and studied in the acquired tomograms (Fig. 1B,D). Transverse lumenal slices of the electron tomograms displayed diagonal electron densities with 8 nm periodicity. The tilt of the striations was reversed on opposing sides of the lumen (arrows in Fig. 1B and Supplementary movie 1), suggesting a left-handed helix with a pitch of 8 nm. We named this structure Tail Axoneme Intra-Lumenal Spiral (TAILS).

To investigate the extent of the TAILS complex, cryo-electron tomograms farther from the tip were examined. A transition from distal singlet microtubules into doublet microtubules was observed in one tomogram, 2.5 μm away from the tip (Fig. 1E,F). In this region, the TAILS structure was still continuous inside all the singlet microtubules and persisted into the doublet microtubules. TAILS eventually terminated approximately 300 nm into the dMT (Fig. 1G). It thus extended for around 3 μm from the spermatozoon tip. A TAILS-like structure was also present in the lumen of the B-tubules, starting from their plus end, and it extended, with its 8 nm periodicity, further towards the sperm head than TAILS in the A-tubule. Closer to the cell body, the A-tubule was filled with less defined electron density.

Intraluminal TAILS-like striations were also found inside central pair microtubules. The distance from the tip at which central pair microtubules terminated was variable between cells. The central pair microtubules stretched through one tomogram acquired at 5.5 μm from the sperm tip (Fig. 1H). In another cryo-ET, acquired closer to the cell body, the central pair microtubules terminated at 7.5 μm from the tail tip. This indicates that central pair microtubules might extend less far than other axonemal microtubules. In both cryo-ETs the TAILS-like striations were found in the central pair microtubules (Supplementary Figure 2). The dMTs did not terminate and did not contain TAILS in either of these tomograms, probably because this occurs closer to the tip, as described above. These results suggest a preference for TAILS to localize towards the microtubule plus ends.

To give an overview of the flagellar regions where TAILS was present, we noted which tomograms it was observed in (Fig. 2). A total of 8 tomograms of known distance from the tail tip presented TAILS. Most of them included microtubules in the singlet region or central pair microtubules within the complete axoneme. On one occasion, TAILS was observed in central pair MTs as far away from the tail tip as >10 μm. Only one tomogram showed the presence of TAILS in doublet microtubules (Fig. 1E–G).

The TAILS complex binds to interior wall of 11 protofilaments with a gap over the seam.
At first sight, it is difficult to see how one might reconcile an 8 nm pitch interior helix with the 12 nm pitch expected at the seam of the 13-protofilaments wall of singlet microtubules (Fig. 3A). To resolve this discrepancy and clarify the nature of the structure, we performed sub-volume alignment and averaging on 1940 particles that were selected along 34 singlet microtubules.
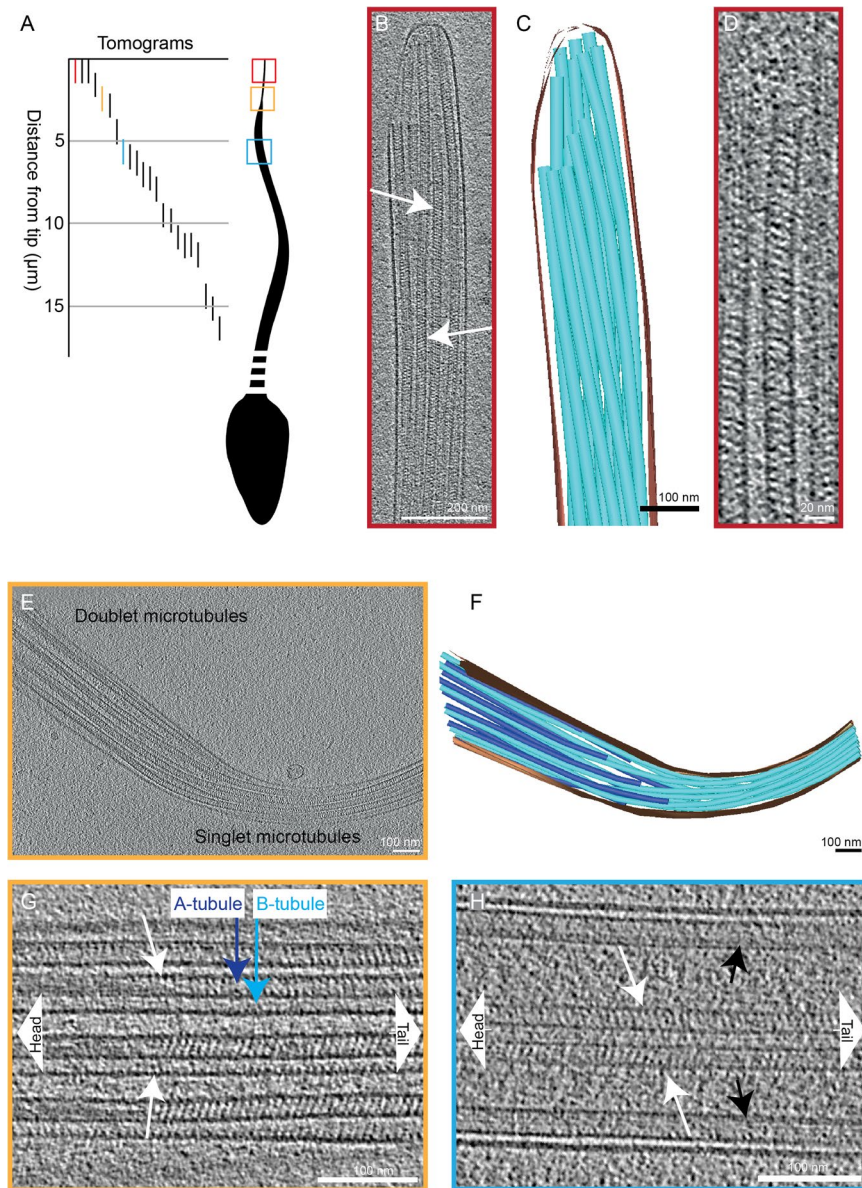
Figure 1. Microtubules in the end piece of the human spermatozoon show a repetitive pattern inside their lumen (**A**) A drawing illustrating positions along the sperm tails where cryo-electron tomograms were acquired. The 22 tomograms shown were acquired on a total of 13 different cells. The highlighted tomograms are shown in the panels with matching colors. (**B**) A 15 nm thick slice from a cryo-electron tomogram of a sperm end piece showing singlet microtubules with repetitive diagonal striations with variable tilt directions (arrows). (**C**) A 3D model of the sperm tip shown in panel B. The microtubules are shown in turquoise, the membrane in brown. (**D**) A 7 nm thick tomogram slice of one singlet microtubule from the sperm end piece in B. (**E**) A tomographic slice showing the transition area from doublet microtubules to singlet microtubules in the sperm tail. (**F**) A 3D model of the sperm tail shown in panel E. The membrane is shown in brown, the A-tubules in turquoise and the B-tubules in blue. (**G**) A tomographic slice showing the end of the intralumenal structure (white arrows) inside the doublet microtubule. (**H**) Central pair microtubules also contain a repetitive structure inside their lumen (white arrows). Black arrows point at doublet microtubules.

Sub-volume averaging increased the signal-to-noise ratio revealing a left-handed interrupted helix. In longitudinal view, TAILS was clearly recognizable as the repetitive pattern seen in the raw data (Fig. 3B,C; Supplementary Movie 2). A 3D model of the sub-tomogram average was created using density thresholding, which also showed the structure of TAILS (Fig. 3D; Supplementary Movie 2). The average showed that TAILS is made up of multiple helical segments. One TAILS segment occurs every 8 nm along the microtubule axis. Each segment has a pitch of 12 nm, matching that of 13 the protofilament microtubule wall (Fig. 3A). This led us to examine the site of TAILS binding in relation to the microtubule seam. The seam could be directly identified in the microtubule lattice (Fig. 3E,F; Supplementary Figure 3).
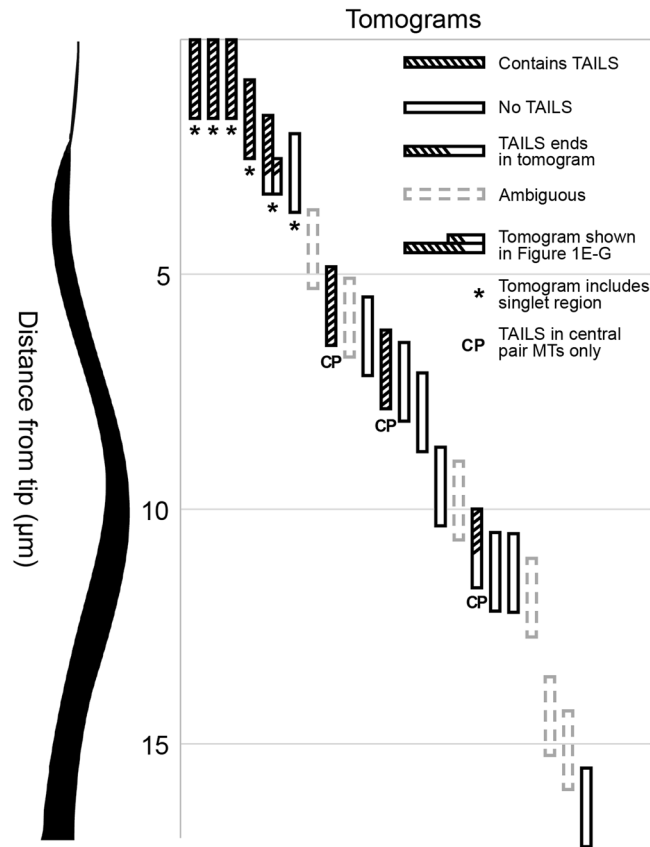
Figure 2. TAILS localize to microtubule plus ends. Each vertical bar represents a tomogram where the presence of the TAILS complex is illustrated with stripes. Empty bars indicate that TAILS was absent and dashed bars indicate that the quality of the tomogram did not allow determination of neither presence nor absence of TAILS. Half-striped bars show that TAILS was partially present. Bars labelled with an asterisk represent that the tomogram included the flagellar singlet region, while bars labelled with CP mean that the data refers to central pair microtubules. On one occasion only (fifth tomogram from the left, also shown in Fig. 1E–G) TAILS was observed in dMTs and it ended halfway through the tomogram.

In cross-sectional view the TAILS complex is clearly visible as an electron density (Fig. 3G) which rotates around the lumen when viewed at successive positions along the microtubule axis (Supplementary Movie 3). Moving through the sub-tomogram average, gaps in the TAILS complexes are apparent on the inside of the microtubule (Fig. 3H-I). Each segment spans between 240 and 305 degrees (based on centers or edges of electron densities, respectively) leaving a gap spanning portions of 2 protofilaments around the MT seam. The proximal end of a given segment occurs at approximately the same axial height as the distal end of the previous segment. The result is a stack of identically oriented, C-shaped segments that are coaxial with the surrounding tubulin helix. TAILS can also be thought of as an interrupted or incomplete 3 start helix, where the interruption is found across the microtubule seam.

Microtubules in the human singlet zone are non-randomly organized. The singlet zone at the flagellum tip appears less highly organized than the complete axoneme, which is more proximal to the cell body. In the human spermatozoa investigated here, the number and position of microtubules are variable both within the singlet zone of an individual single sperm tail, and between singlet zones of different sperm tails. The disruption of TAILS decoration over the MT seam can be used as a compass to investigate whether or not microtubule seams in the singlet region are randomly oriented with respect to each other.

Three cryo-ETs of singlet regions containing 9, 11 and 14 microtubules were investigated, two were acquired at the absolute tip of the sperm tail and one at 1.5 µm from the tip (Fig. 4A). The presence of 14 singlet microtubules in one cryo-ET is noteworthy since it shows that both A- and B- tubules nucleate singlet microtubules. All of these microtubules consisted of 13 protofilaments, meaning that the incomplete B-tubule gained 3 protofilaments after separating from the A-tubule. Using the coordinates applied to rotate particles and generate the sub-tomogram average, the 3D isosurface models of singlet microtubules could be docked back into a 3D model representing the microtubule orientation inside each cell, allowing easy visualization of the seam orientations (Fig. 4B–D).

To investigate possible non-randomness of singlet region seam orientations, bootstrap analysis was performed using a number of local and global measures of orientation. Local measures, such as mean or minimum angular distance to neighboring tubules, showed no indication of non-randomness. A more global measure, total change in angle for a path visiting each microtubule exactly once, does however suggest partial ordering. Bootstrapped
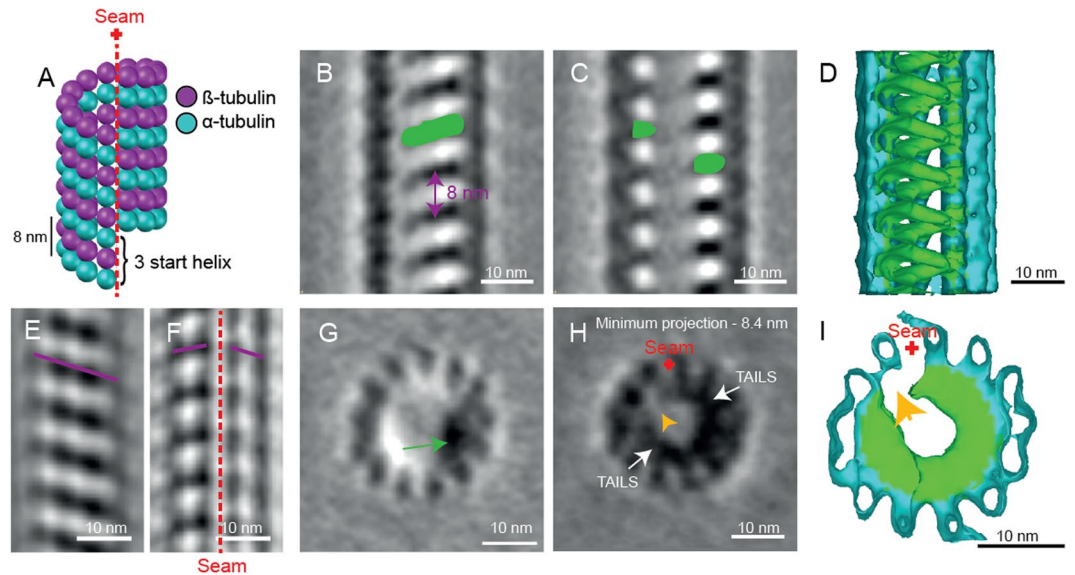
Figure 3. Sub-tomogram averaging reveals the TAILS complex, an interrupted left-handed helix that follows the pattern of the internal microtubule lattice. (**A**) Cartoon of a typical 13 protofilament microtubule with the 3 start helix and a 12 nm pitch. The microtubule seam is marked with the red dotted line. (**B,C**) 0.7 nm thick longitudinal slices through the sub-tomogram average showing the microtubule lattice and the internal electron density (green). (**D**) The 3D model shows the microtubule lattice (turquoise) and the intralumenal structure (green). Some protofilaments have been cut away from the model to reveal the internal helical structure. (**E**) A 4 nm thick slice of the sub-tomogram average shows a B-lattice arrangement of the tubulin heterodimers (purple line). (**F**) A 4 nm thick slice of the sub-tomogram average shows a disruption in the microtubule B-lattice, revealing the location of the seam (red dotted line). (**G**) A 0.7 nm thick cross-sectional view of the sub-tomogram average. The green arrow points at the electron density of TAILS. View from flagellum tip, looking towards sperm head. (**H**) Projection of a 8.4 nm thick cross-sectional view of the sub-tomogram average showing the end of one TAILS complex segment, the beginning of the next and the gap between them (yellow arrow). (**I**) 3D model of the microtubule (turquoise) and the TAILS complex (green) reveals the gap (yellow arrow) in the TAILS complex.
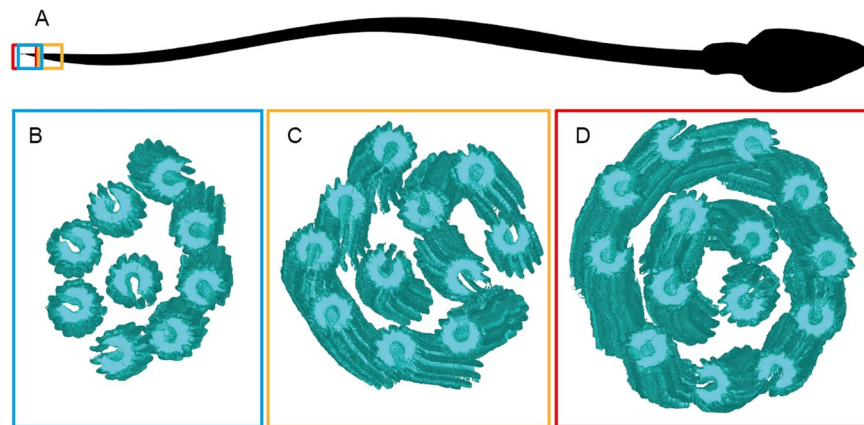
Figure 4. Microtubules in the singlet region vary in number but are non-randomly oriented. (**A**) A cartoon of a spermatozoon showing the location of the cryoETs shown in (**B**–**D**) Isosurfaces of sub-tomogram averaged singlet microtubules were aligned into a model volume according to their original orientations. The gap in the microtubules is used as a marker of the microtubule seam. Three singlet regions with (**A**) 9 (**B**) 11 and (**C**) 14 microtubules were analyzed and showed a non-random orientation of the seam.

p-value estimates of 0.011, 0.301, and 0.031 were obtained for singlet zones with 9, 11, and 14 microtubules, respectively. Combined data from all 3 singlet zones yields a highly significant p-value ($\leq$0.005), as described in Materials and Methods, indicating that seam orientations are not completely random. We suggest that the observed deviations from randomness likely reflect remnants of the more rigid organization of the proximal axoneme.

The seam is located between protofilaments A8 and A9 of the doublet microtubules. Since the position of the A-tubule seam in dMTs has not been resolved using cryo-ET, and other methods such as single particle analysis have given conflicting results[9–11], there is still some debate as to where it is localized. The orientation of the gap in TAILS can be used as an indicator of the microtubule seam position in dMTs.

In two cryo-ETs that we acquired, the transition from dMTs to singlets was included in the volume. The TAILS complex clearly extended into dMTs in one of these tomograms (Fig. 1G). In the other cryo-ET, the TAILS complex in the A-tubule was not visible but B-tubules still had clear luminal decorations. This shows that the extent of the TAILS complex within dMTs is variable. Only the tomogram with complete TAILS decoration in both dMTs (478 particles) was used for sub-tomogram averaging. The structure has an 8 nm repeat, like in singlet microtubules, and a gap of the TAILS complex was found to be at the outer junction between protofilament A8 and A9 of the dMTs (Fig. 5A–F; Supplementary Movie S4). Thus, we inferred that this is the position of the A-tubule seam. Inside the B-tubule seven or eight protofilamens were decorated, possibly with a TAILS-like protein, but protofilaments B1, B10 and possibly B9 were undecorated.

Sub-tomogram averaging enabled to increase the signal to noise ratio to the point where the α and β tubulins were resolved in our dMTs (Fig. 5H). The seam was clearly visible between protofilament A8 and A9 (Fig. 5G–I), in the outer junction of the dMT. In comparison, the dMT inner junction showed a perfect B-lattice (Fig. 5J).

Tubulin heterodimers were equally spaced 8 nm apart, but there appeared to be a compaction of their electron densities that may or may not be TAILS related.

Discussion

This is the first time an intact human flagellum has been studied using cryo-electron tomography. We have described a novel structure that we named TAILS, which is comprised of helical segments spaced every 8 nm. Many TAILS segments assemble into an array along several micrometers of the inner wall of all singlet microtubules in the end piece of human sperm tails. TAILS binds to the inside of the tubulin heterodimers and spans 11 protofilaments. The interruption of the helix spans over the position of the microtubule seam. TAILS has a pitch and handedness matching that of the tubulin helices comprising the microtubule wall. This pattern is consistent with what would be expected for a structure comprised of repeating identical segments or subunits capable of distinguishing between α and β tubulin. We suggest two alternative models for the molecular structure of TAILS, which could consist of multiple monomeric segments (Fig. 6A) or multiple groups of 11 subunits (Fig. 6B), leaving a gap over the seam in either case. Our sub-tomogram averaging yielded a resolution that was high enough to distinguish some of the tubulin subunits on the dMTs still inside of the frozen cell in its native state. The gaps between heterodimers have previously been shown to be larger than those between the subunits of each dimer[42], therefore we consider it most likely that this gap in the microtubule lattice occurs in between heterodimers. We infer the identity of the tubulin subunits with the help of the following information: (1) microtubule plus end is capped with the β-tubulin subunit[43], and (2) flagella have their microtubule plus ends at the flagellum tip[9,44]. TAILS binds in the interface between the α and β tubulin subunits, and extends with a slight slope towards the microtubule plus end (Fig. 5G and K,L).

The achieved resolution allowed identification of the seam in both singlets and dMTs, making this the first time this structure has been visualized directly inside an intact cell. The reported position of the seam in dMTs differs with previously published papers. First, the seam was inferred to be at the inner junction of the dMTs of sea urchin sperm (*Psammechinus miliaris*)[9], then two more recent papers, using single particle techniques to achieve high resolution maps of dMTs from *Tetrahymena thermophila*, suggested a position of the seam at the outer junction, between protofilaments A9–10[11] or A10–11[10]. We observed the seam between the A8–9 protofilaments, both by the location of the gap in TAILS and by direct visualization. The differences observed might be a result of using different methods, or might reflect a real difference in the location of the seam between species.

The presence of 14 microtubules in the singlet region confirms that also in humans, the dMTs can split and form a duplex microtubule, like the ones seen in rodent spermatozoa[16]. The 13 protofilament microtubule lattice found *in vivo* has been shown to be determined by the nucleation factor γ tubulin ring complex (γ-TuRC)[45]. The fact that all the singlet microtubules consist of 13 protofilaments, even those derived from the 10 protofilaments B-tubule, suggests that γ-TuRC is not the sole determinant of protofilament number *in vivo*. The orientation preference of the microtubules in the singlet zone suggests that the singlets maintain the seam position previously established in the complete axoneme.

TAILS decorates the inside of every tubulin heterodimer, except the two protofilaments at the seam, for several micrometers before the microtubule plus ends. The function of this complex structure is of course of high interest. Since no other human flagellum tip have been examined with electron tomography or cryoEM, it is unclear if TAILS is a sperm-specific structure and if it has a sperm-specific function. We suggest four different hypotheses for its function, which are not mutually exclusive. First, TAILS seems to have compacted the tubulin heterodimer, a feature which would translocate to the outside of the microtubule. This rearrangement of the lattice might prevent motor proteins and other MAPs to bind in their regular way, defining the singlet region in a molecular manner. Second, TAILS might provide extra rigidity to the microtubules in this region, so that the end piece has an increased stiffness, which might aid motility, crucial to spermatozoa. It may provide a structural support such as the para-flagellar rod in *Trypanosoma brucei*[46–48], another single cell whose motility is crucial for its survival[49]. Third, the TAILS complex could also stabilize microtubules, preventing the dynamic turnover constantly occurring in flagella tips[50]. Helical reinforcement is an efficient solution regularly used in engineering, *e.g.* in bicycle frame tubes or in armored hoses. Since microtubules depolymerize by outward curling of protofilaments[51,52], the c-shaped helical segments of TAILS could prevent splaying similar to how spiral hose reinforcement prevents radial expansion. The saved energy could then instead be invested in rapid cellular translocation. This hypothesis is consistent with the observation that the TAILS complexes extend to the central pair microtubules, far into the sperm tail. Lastly, TAILS might also play a role in determining the direction in which spermatozoa swim, since
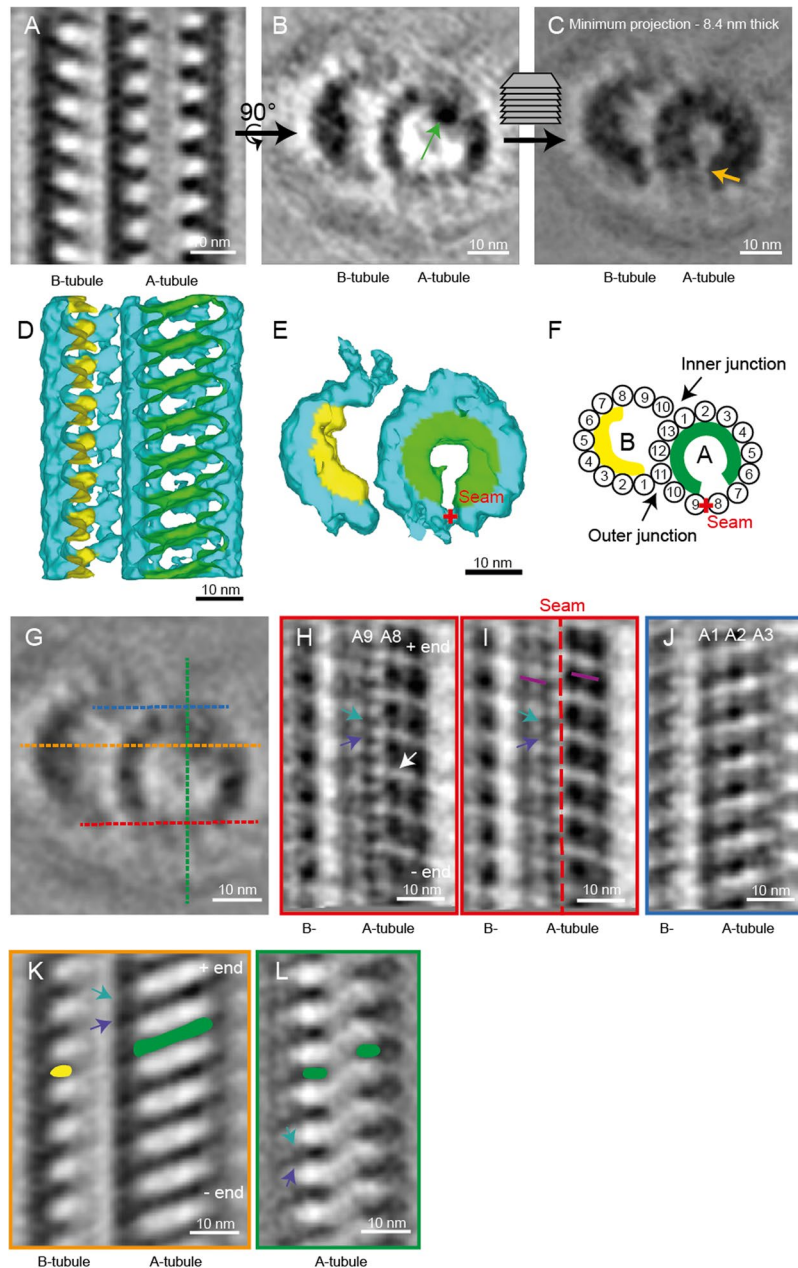
Figure 5. TAILS binds to the interphase between α and β tubulin in doublet microtubules. The A-tubule seam is found between protofilaments A8 and A9. (**A**) Longitudinal section through a sub-tomogram average of a dMT showing an 8 nm repeat structure on the inside of the microtubule walls. (**B**) TAILS is seen as an electron dense dot in one cross-section of the average (green arrow). (**C**) Minimum projection over an 8.4 nm-thick cross-section showing the expansion of TAILS over 11 protofilaments and the gap in the structure (yellow arrow). (**D**) Isosurface model of the averaged dMT: tubulin in turquoise, TAILS in green and B-tubule decorations in yellow. The front microtubule wall was removed for better visualization. (**E**) Cross-sectional view of the isosurface from the plus end. The red cross highlights the position of the seam. (**F**) A cartoon of the dMT with protofilament numbers, the seam (red cross) and TAILS (green). (**G**) Cross-sectional view showing the location of the (**H–K**) longitudinal views with color-labelled section lines. (**H**) 0.7 nm-thick tangential slice of the average, showing the microtubule lattice from the outside. The subunits of the tubulin heterodimer were resolved (resolution <4 nm). Knowing the position of the MT plus end and that of the gap (white arrow) in the lattice, we infer the position of α (purple arrow) and β (turquoise arrow). (**I**) 4 nm-thick slice of the average contains whole protofilaments and reveals the position of the A-tubule seam (red dotted line). The slope of the B-lattice is visualized on both sides of the seam (purple lines). (**J**) 4 nm-thick slice of the dMT sub-tomogram average, seen from the inner junction, showing a perfect B-lattice arrangement over protofilaments A1, A2, and A3. (**K**) TAILS (in green) binds between the α and β subunits. The decoration within the B tubule is marked in yellow. (**L**) TAILS binds to the interface between the α and β subunit.
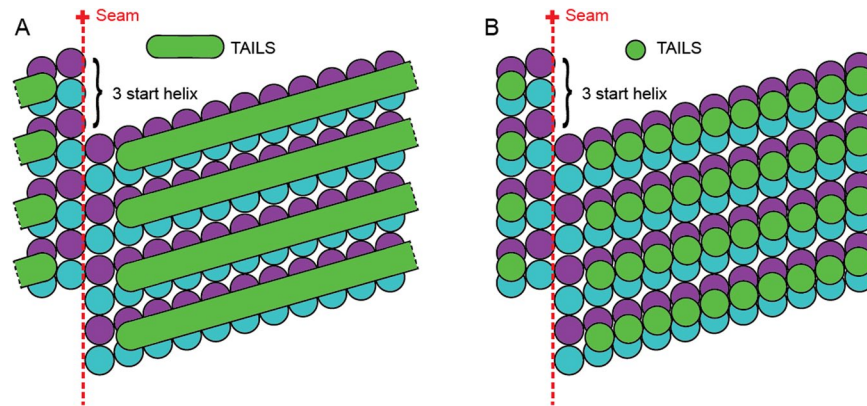
Figure 6. A schematic representation of two different models of the molecular structure of TAILS. A 13-protofilaments microtubule from the sperm tail tip is shown as opened up and unfolded into a sheet, viewed from the lumenal side. The TAILS complex (green) is placed at the position along the y-axis as found in dMTs, as we do not know the exact location in singlet microtubules. The α and β tubulin subunits are shown in blue and purple respectively. (**A**) TAILS is drawn as monomeric C-shaped segments that bind to each protofilament at the intraheterodimer interface, leaving a gap over the seam. (**B**) TAILS is drawn as a series of C-shaped multimeric segments, each formed by 11 subunits.

there is evidence in other organisms that the singlet zone may be associated with signaling or sensory functions as well as motility[4]. Future studies will determine if TAILS is sperm-specific or a general structure of human flagella, which would aid in understanding its function.

Potential mechanisms for controlling the extent and orientation of the helical segments are worth considering. The TAILS complex has a gap in the structure spanning the inside of the microtubule seam. Binding specificity of the putative inner wall binding monomers coupled with conformational variation of the subunits closest to the seam alone could account for the observed structure. A monomer binding to the alpha and beta tubulin interface, like TAILS, could be unable to bind to the intraheterodimer interface across the seam, leaving a gap. If a bridge over this gap is present, such a structure would likely be comprised of protein(s) distinct from the inner wall binding monomers, and its length might naturally limit the span of the helical segments.

In conclusion, we performed cryo-electron microscopy and tomography on intact human spermatozoa. This study led to the discovery of a novel, complex structure inside of the microtubule lumen which we named TAILS. The structure extended for several micrometers along microtubules at their plus end, in the flagellum tip, and bound microtubules at the inner intradimer interface of tubulin dimers, but left a gap over the seam. We hypothesized that TAILS might have a role in tubulin compaction, flagellar rigidity, microtubule stability and/or directionality of cellular translocation.

Since sperm motility and morphology are determinants of male fertility[53], understanding the functional role of the TAILS complex may have clinical implications relating to male infertility and contraception. Our discovery of a novel extensive microtubule associated structure, despite the fact that microtubules have been studied for over 50 years, underlines the importance of studying human microtubules and flagella, as well as other organisms, by cryo-ET.

We look forward to the future identification of the proteins involved in regulating the microtubule cytoskeleton from the lumenal side, including the proteins forming the TAILS complex.

Materials and Methods

Sample collection and plunge freezing. Spermatozoa were donated by three healthy men and frozen unperturbed in seminal fluid to which colloidal gold was added (to be used as fiducial markers). A Vitrobot climate-controlled plunge freezer (FEI Company Ltd., Eindhoven, The Netherlands) was used within 1–3 h post ejaculation. After freezing for electron microscopy, remaining cells were examined under the light microscope, where their motility ensured that viable spermatozoa had been frozen.

Cryo-electron microscopy and tomography. Microscopy was performed as described previously[46,54]. In brief, images (electron dose of ~25 e⁻/Å²; −4 to −6 µm defocus) were acquired at 27500 x on a Tecnai F30 electron microscope (FEI Company Ltd) operated at 300 kV. The detector was a GATAN UltraCam, lens-coupled, 4 K CCD camera (binned by 2) attached to a Tridiem Gatan Image Filter (GIF: operated at zero-loss mode with an energy window of 20 eV; Gatan Inc., Pleasanton, CA, USA). For tomography, tilt-series were acquired every 1.5 degree (±60 degrees) using serialEM software[55]. The total electron dose was kept between 80–120 e⁻/Å². Cryo-ETs were calculated using eTomo and CTF correction was applied to all datasets. All tomograms were acquired on cells from a single donor and cryo-electron micrographs were acquired from the other two donors to confirm the presence of TAILS.

Subvolume Alignment and Averaging. Models with open contours approximating the path of microtubules in the electron tomograms were created in IMOD[56]. PEET[33] was used for adding model points with the desired spacing (8 nm, matching the periodicity of the TAILS complex) along each contour and for subsequent

alignments and averages. For each model point a subvolume of 60 voxel^3 (46.2 nm^3) was selected. Number of tomograms, microtubules and particles for each average can be found in Table 1. Subvolumes from individual microtubules were first aligned and averaged separately. Final alignment and averaging combining microtubules and tomograms was then performed starting from positions and orientations obtained by aligning the individual tube averages. Soft-edge cylindrical masks with empirically chosen radii were applied during alignment of singlet microtubules. Wedge-mask compensated principal component analysis followed by k-means clustering[57] was used to check for heterogeneity and to assess the impact of missing wedge artifacts on candidate alignments.

Statistical Analysis of the Singlet Region. Volumetric and isosurface representations corresponding to each tomogram were constructed by pasting the final average and its 3D model back into the original volumes. Statistical analysis of microtubule azimuthal positions was conducted in MATLAB (The Mathworks Inc., Natick, MA) using bootstrap analysis with 10,000 replicates and, when necessary, bounded depth-first search to compute the optimal value of the statistic of interest for each bootstrap replicate. As a global measure for higher-order organization, we used bounded depth-first search to compute, for each spermatozoon, the length of the minimum angular distance path visiting each singlet microtubule exactly once. An overall probability of finding non-random orientation of microtubules based on data from all three spermatozoa was calculated. The p-values for each spermatozoon were combined using Fisher's method for independent hypothesis tests[58,59]. Alternatively, we can also arrive at an overall p-value by bootstrapping the mean or, equivalently, the sum of the 3 minimum path lengths.

Data availability. The datasets generated and analysed during the current study are available from the corresponding author upon request.

Ethics statement. According to the NIH self-test and instructions (https://humansubjects.nih.gov/questionnaire), our study does not classify as research on human subjects and it was therefore exempt from ethical approval for the following reasons: (1) this study involved *only* the use of secondary analysis of biological material not collected specifically for this study, and (2) the samples were provided without identifiable information by someone without any role in this research study except providing.

References

1. Hilgendorf, K. I., Johnson, C. T. & Jackson, P. K. ScienceDirect The primary cilium as a cellular receiver: organizing ciliary GPCR signaling. *Current Opinion in Cell Biology* **39**, 84–92 (2016).
2. Praveen, K., Davis, E. E. & Katsanis, N. Unique among ciliopathies: primary ciliary dyskinesia, a motile cilia disorder. *F1000Prime Rep* **7** (2015).
3. Afzelius, B. A., Dallai, R., Lanzavecchia, S. & Bellon, P. L. Flagellar structure in normal human spermatozoa and in spermatozoa that lack dynein arms. *Tissue Cell* **27**, 241–247 (1995).
4. Fisch, C. & Dupuis-Williams, P. Ultrastructure of cilia and flagella - back to the future! *Biology of the Cell* **103**, 249–270 (2011).
5. Nicastro, D. *et al.* Cryo-electron tomography reveals conserved features of doublet microtubules in flagella. *Proceedings of the National Academy of Sciences* **108**, E845–53 (2011).
6. Mandelkow, E. M., Schultheiss, R., Rapp, R., Müller, M. & Mandelkow, E. On the surface lattice of microtubules: helix starts, protofilament number, seam, and handedness. *J. Cell Biol.* **102**, 1067–1073 (1986).
7. Kikkawa, M., Ishikawa, T., Nakata, T., Wakabayashi, T. & Hirokawa, N. Direct visualization of the microtubule lattice seam both *in vitro* and *in vivo*. *J. Cell Biol.* **127**, 1965–1971 (1994).
8. McIntosh, J. R., Morphew, M. K., Grissom, P. M., Gilbert, S. P. & Hoenger, A. Lattice Structure of Cytoplasmic Microtubules in a Cultured Mammalian Cell. *Journal of Molecular Biology* **394**, 177–182 (2009).
9. Song, Y. H. & Mandelkow, E. The anatomy of flagellar microtubules: polarity, seam, junctions, and lattice. *J. Cell Biol.* **128**, 81–94 (1995).
10. Maheshwari, A. *et al.* a- and b-Tubulin Lattice of the Axonemal Microtubule Doublet and Binding Proteins Revealed by Single Particle Cryo-Electron Microscopy and Tomography. *Structure/Folding and Design* **23**, 1584–1595 (2015).
11. Ichikawa, M. *et al.* Subnanometre-resolution structure of the doublet microtubule reveals new classes of microtubule-associated proteins. *Nature Communications* **8**, 1–12 (2017).
12. Ringo, D. L. Flagellar motion and fine structure of the flagellar apparatus in Chlamydomonas. *J. Cell Biol.* **33**, 543–571 (1967).
13. Satir, P. Studies on cilia. 3. Further studies on the cilium tip and a 'sliding filament' model of ciliary motility. *J. Cell Biol.* **39**, 77–94 (1968).
14. Höög, J. L. *et al.* Modes of flagellar assembly in Chlamydomonas reinhardtii and Trypanosoma brucei. *eLife* **3**, e01479 (2014).
15. Woolley, D., Gadelha, C. & Gull, K. Evidence for a sliding-resistance at the tip of the trypanosome flagellum. *Cell Motil. Cytoskeleton* **63**, 741–746 (2006).
16. Woolley, D. M. & Nickels, S. N. Microtubule termination patterns in mammalian sperm flagella. *J. Ultrastruct. Res.* **90**, 221–234 (1985).
17. Nogales, E. & Zhang, R. ScienceDirectVisualizing microtubule structural transitions and interactions with associated proteins. *Current Opinion in Structural Biology* **37**, 90–96 (2016).
18. Howard, J. & Hyman, A. A. Microtubule polymerases and depolymerases. *Current Opinion in Cell Biology* **19**, 31–35 (2007).
19. Akhmanova, A. & Steinmetz, M. O. Control of microtubule organization and dynamics: two ends in the limelight. *Nat Rev Mol Cell Biol* **16**, 711–726 (2015).
20. Perez, F., Diamantopoulos, G. S., Stalder, R. & Kreis, T. E. CLIP-170 highlights growing microtubule ends *in vivo*. *Cell* **96**, 517–527 (1999).
21. Mimori-Kiyosue, Y., Shiina, N. & Tsukita, S. The dynamic behavior of the APC-binding protein EB1 on the distal ends of microtubules. *Curr. Biol.* **10**, 865–868 (2000).
22. Nakaseko, Y., Goshima, G., Morishita, J. & Yanagida, M. M phase-specific kinetochore proteins in fission yeast: microtubule-associating Dis1 and Mtc1 display rapid separation and segregation during anaphase. *Curr. Biol.* **11**, 537–549 (2001).
23. Goodwin, S. S. & Vale, R. D. Patronin Regulates the Microtubule Network byProtecting Microtubule Minus Ends. *Cell* **143**, 263–274 (2010).
24. Kollman, J. M., Polka, J. K., Zelter, A., Davis, T. N. & Agard, D. A. Microtubule nucleating γ-TuSC assembles structures with 13-fold microtubule-like symmetry. *Nature* **466**, 879–882 (2010).
25. Oakley, C. E. & Oakley, B. R. Identification of gamma-tubulin, a new member of the tubulin superfamily encoded by mipA gene of Aspergillus nidulans. *Nature* **338**, 662–664 (1989).

26. Chan, J., Jensen, C. G., Jensen, L. C., Bush, M. & Lloyd, C. W. The 65-kDa carrot microtubule-associated protein forms regularly arranged filamentous cross-bridges between microtubules. *Proc. Natl. Acad. Sci. USA* **96**, 14931–14936 (1999).
27. Kellogg, E. H. *et al.* Near-atomic cryo-EM structure of PRC1 bound to the microtubule. *Proceedings of the National Academy of Sciences* **113**, 9430–9439 (2016).
28. Scheffler, K., Minnes, R., Fraisier, V., Paoletti, A. & Tran, P. T. Microtubule minus end motors kinesin-14 and dynein drive nuclear congression in parallel pathways. *J. Cell Biol.* **209**, 47–58 (2015).
29. Teng, J. *et al.* Synergistic effects of MAP2 and MAP1B knockout in neuronal migration, dendritic outgrowth, and microtubule organization. *J. Cell Biol.* **155**, 65–76 (2001).
30. Zanic, M., Widlund, P. O., Hyman, A. A. & Howard, J. ncb2744. *Nat Cell Biol* **15**, 688–693 (2013).
31. Kar, S., Fan, J., Smith, M. J., Goedert, M. & Amos, L. A. Repeat motifs of tau bind to the insides of microtubules in the absence of taxol. *EMBO J.* **22**, 70–77 (2003).
32. Soppina, V., Herbstman, J. F., Skiniotis, G. & Verhey, K. J. Luminal Localization of α-tubulin K40 Acetylation by Cryo-EM Analysis of Fab-Labeled Microtubules. *PLoS ONE* **7**, e48204 (2012).
33. Nicastro, D. The Molecular Architecture of Axonemes Revealed by Cryoelectron Tomography. *Science* **313**, 944–948 (2006).
34. Schwartz, C. L., Heumann, J. M., Dawson, S. C. & Hoenger, A. A Detailed, Hierarchical Study of Giardia lamblia's Ventral Disc Reveals Novel Microtubule-Associated Protein Complexes. *PLoS ONE* **7**, e43783 (2012).
35. Dentler, W. L. Structures linking the tips of ciliary and flagellar microtubules to the membrane. *J. Cell. Sci.* **42**, 207–220 (1980).
36. Rodríguez Echandía, E. L., Piezzi, R. S. & Rodríguez, E. M. Dense-core microtubules in neurons and gliocytes of the toad Bufo arenarum Hensel. *Am. J. Anat.* **122**, 157–166 (1968).
37. Vaughan, S., Shaw, M. & Gull, K. A post-assembly structural modification to the lumen of flagellar microtubule doublets. *Curr. Biol.* **16**, R449–50 (2006).
38. Höög, J. L. *et al.* Organization of interphase microtubules in fission yeast analyzed by electron tomography. *Dev. Cell* **12**, 349–361 (2007).
39. Garvalov, B. K. *et al.* Luminal particles within cellular microtubules. *J. Cell Biol.* **174**, 759–765 (2006).
40. Sui, H. & Downing, K. H. Molecular architecture of axonemal microtubule doublets revealed by cryo-electron tomography. *Nature* **442**, 475–478 (2006).
41. Brown, J. R., Schwartz, C. L., Heumann, J. M., Dawson, S. C. & Hoenger, A. Journal of Structural Biology. *J. Struct. Biol.* **194**, 38–48 (2016).
42. Alushin, G. M. *et al.* High-Resolution Microtubule Structures Reveal the Structural Transitionsin ab-Tubulin upon GTP Hydrolysis. *Cell* **157**, 1117–1129 (2014).
43. Mitchison, T. J. Localization of an exchangeable GTP binding site at the plus end of microtubules. *Science* **261**, 1044–1047 (1993).
44. Euteneuer, U. & McIntosh, J. R. Polarity of some motility-related microtubules. *Proc. Natl. Acad. Sci. USA* **78**, 372–376 (1981).
45. Moritz, M., Braunfeld, M. B., Sedat, J. W., Alberts, B. & Agard, D. A. Microtubule nucleation by gamma-tubulin-containing rings in the centrosome. *Nature* **378**, 638–640 (1995).
46. Höög, J. L., Bouchet-Marquis, C., McIntosh, J. R., Hoenger, A. & Gull, K. Cryo-electron tomography and 3-D analysis of the intact flagellum in Trypanosoma brucei. *J. Struct. Biol.* **178**, 189–198 (2012).
47. Portman, N. & Gull, K. The paraflagellar rod of kinetoplastid parasites: From structure to components and function. *International Journal for Parasitology* **40**, 135–148 (2010).
48. Koyfman, A. Y. *et al.* Structure of Trypanosoma brucei flagellum accounts for its bihelical motion. *Proc. Natl. Acad. Sci. USA* **108**, 11105–11108 (2011).
49. Broadhead, R. *et al.* Flagellar motility is required for the viability of the bloodstream trypanosome. *Nature* **440**, 224–227 (2006).
50. Marshall, W. F. Intraflagellar transport balances continuous turnover of outer doublet microtubules: implications for flagellar length control. *J. Cell Biol.* **155**, 405–414 (2001).
51. Simon, J. R. & Salmon, E. D. The structure of microtubule ends during the elongation and shortening phases of dynamic instability examined by negative-stain electron microscopy. *J. Cell. Sci.* **96**(Pt 4), 571–582 (1990).
52. Mandelkow, E. M., Mandelkow, E. & Milligan, R. A. Microtubule dynamics and microtubule caps: a time-resolved cryo-electron microscopy study. *J. Cell Biol.* **114**, 977–991 (1991).
53. Esteves, S. C. Novel concepts in male factor infertility: clinical and laboratory perspectives. *Journal of Assisted Reproduction and Genetics* 1–17 https://doi.org/10.1007/s10815-016-0763-8 (2016).
54. Höög, J. L. & Lötvall, J. Diversity of extracellular vesicles in human ejaculates revealed by cryo-electron microscopy. *Journal of Extracellular Vesicles* **4** (2015).
55. Mastronarde, D. N. Automated electron microscope tomography using robust prediction of specimen movements. *J. Struct. Biol.* **152**, 36–51 (2005).
56. Kremer, J. R., Mastronarde, D. N. & McIntosh, J. R. Computer visualization of three-dimensional image data using IMOD. *J. Struct. Biol.* **116**, 71–76 (1996).
57. Heumann, J. M., Hoenger, A. & Mastronarde, D. N. Journal of Structural Biology. *J. Struct. Biol.* **175**, 288–299 (2011).
58. Fischer, R. A. *Statistical methods for Research Workers.* (Oliver and Boyd 1925).
59. Frederick, M. & Fischer, R. A. Questions and answers. *The American Statestician* **2**, 30–31 (1948).

Acknowledgements

Author Contributions

Experimental design: J.L.H., P.O.W. Acquisition of cryo-electron micrographs: J.L.H., G.M. Acquisition of cryo-electron tomograms: J.L.H., C.L.S. Calculation and modelling of tomograms: J.L.H., D.Z. Sub-tomogram averaging and processing of data: J.M.H., D.Z. and A.S.S. Writing of manuscript: J.M.H., P.O.W., D.Z. and J.L.H.

Additional Information

Supplementary information accompanies this paper at https://doi.org/10.1038/s41598-018-21165-8.

Competing Interests: The authors declare no competing interests.

Publisher's note: Springer Nature remains neutral with regard to jurisdictional claims in published maps and institutional affiliations.